A volcano bursting at the seams: Inflation, faulting, and eruption at Sierra Negra volcano, Galápagos

William W. Chadwick Jr. Oregon State University–National Oceanographic and Atmospheric Administration, 2115 SE OSU Drive, Newport, Oregon 97365, USA
Dennis J. Geist Geological Sciences, University of Idaho, Moscow, Idaho 83844, USA
Sigurjón Jónsson Institute of Geophysics, ETH Zürich, Schafmattstrasse 30, 8093 Zürich, Switzerland
Michael Poland Hawaii Volcano Observatory, U.S. Geological Survey, P.O. Box 51, Hawaii National Park, Hawaii 96718, USA
Daniel J. Johnson* Department of Geology, University of Puget Sound, Tacoma, Washington 98416, USA
Charles M. Meertens UNAVCO, 6350 Nautilus Drive, Boulder, Colorado 80301, USA

ABSTRACT

The results of geodetic monitoring since 2002 at Sierra Negra volcano in the Galápagos Islands show that the filling and pressurization of an ~2-km-deep sill eventually led to an eruption that began on 22 October 2005. Continuous global positioning system (CGPS) monitoring measured >2 m of accelerating inflation leading up to the eruption and contributed to nearly 5 m of total uplift since 1992, the largest precursory inflation ever recorded at a basaltic caldera. This extraordinary uplift was accommodated in part by repeated trapdoor faulting, and coseismic CGPS data provide strong constraints for improved deformation models. These results highlight the feedbacks between inflation, faulting, and eruption at a basaltic volcano, and demonstrate that faulting above an intruding magma body can relieve accumulated strain and effectively postpone eruption.

Keywords: inflation, intrusion, geodesy, global positioning system, interferometric synthetic aperture radar.

INTRODUCTION

Most of what geologists understand about igneous intrusion comes from uplifted and exhumed ancient rocks (Breitkreuz and Petford, 2004; Marsh, 2004). However, this information is usually complex because it represents a time-integrated record that is overprinted by unrelated geologic processes. More direct observations come from active volcanoes where modern seismic and geodetic data can reveal the mechanics and time scales of intrusion, as well as causal links to eruptions (Chouet, 2003; Dzurisin, 2003). Here we describe the results of a geodetic study of Sierra Negra volcano in the Galápagos Islands that reveal the filling of a shallow sill, how the volume of this intrusion was accommodated, and the feedbacks between intrusion, faulting, and eruption. We demonstrate that the filling and pressurization of this sill eventually led to an eruption that commenced on 22 October 2005. This is the first pre-eruption sequence ever monitored at a Galápagos volcano with global positioning system (GPS), and it provides strong constraints for deformation models that differ from those of previous studies.

DEFORMATION MONITORING AT SIERRA NEGRA

Sierra Negra, a basaltic volcano with a large summit caldera, is the largest volcano in the Galápagos (Fig. 1) and last erupted in 1979 (Reynolds and Geist, 1995). Prior to 2000, deformation monitoring in the Galápagos was limited to satellite radar interferometry (InSAR), which combines radar images from two satellite passes to measure changes in the range between the satellite and the Earth's surface. Results from three different intervals during the 1990s showed that the caldera floor of Sierra Negra volcano inflated by 2.7 m between 1992 and 1999 (Fig. 1D) (Amelung et al., 2000; Yun et al., 2006). From 1992 to 1997, the pattern of inflation was nearly axisymmetric and mostly limited to the caldera floor; the maximum uplift was near the center of the caldera. This was modeled as due to intrusion of magma into a sill beneath the caldera at a depth of ~2 km (Amelung et al., 2000; Jónsson et al., 2005). In contrast, between 1997 and 1998 the maximum uplift was centered on the southern limb of a preexisting intracaldera fault system (Fig. 1B). The shift was interpreted as being due to ~1.2 m of slip along a steeply south-dipping normal fault (Amelung et al., 2000; Jónsson et al., 2005). The focus of inflation at Sierra Negra shifted back to the center of the caldera between 1998 and 1999, again interpreted as magma filling a subcaldera sill (Amelung et al., 2000).

Campaign GPS monitoring of Sierra Negra began in 2000 and during 2000–2002 showed a striking deceleration in the uplift rate previously documented by InSAR, followed by a change to subsidence of ~9 cm/yr (Fig. 1D) (Geist et al., 2006). The deflationary source was modeled as a contracting sill at a depth of 2.1 km, similar to the inflationary source of the 1990s (Amelung et al., 2000). Microgravity measurements over the same interval point to either downward magma withdrawal or segregation of bubbles from vesiculated magma as causes for contraction of the sill (Geist et al., 2006).

In June 2002, a six station continuous global positioning system (CGPS) network was deployed at Sierra Negra (Fig. 1B; GSA Data Repository[1]). The CGPS data were processed using the BERNESE software (Hugentobler et al., 2001). The CGPS network consists of four single-frequency and two dual-frequency instruments; two of the stations are near the previous centers of inflation and trapdoor faulting (GV02 and GV06, respectively). From June 2002 to April 2003, the caldera floor continued the subsidence that had begun in 2000–2001. In April 2003, deformation of the caldera floor changed from deflation to inflation (Figs. 1E, 1F). The rate of inflation gradually increased throughout 2004 and into 2005. Between 1 April 2003 and 15 April 2005, station GV02 was uplifted a total of 89 cm, accompanied by 69 cm of horizontal extension across the caldera (GV03–GV06).

Elastic inflation was interrupted by an episode of inelastic trapdoor faulting marked by an m_b4.6 earthquake on 16 April 2005 (National Earthquake Information Center; http://neic.usgs.gov). The displacements associated with this faulting event were documented in extraordinary detail by the CGPS network. An epoch-by-epoch kinematic solution of the position of GV06 on 16 April 2005 shows that it was uplifted by 84 cm within 10 s (Fig. 1F), and the cross-caldera line contracted by 26 cm.

The rate of inflation did not appear to be affected by the faulting event of 16 April 2005 and continued its upward trend, eventually approaching rates of 1 cm/day at stations GV02 and GV04 (Fig. 1). We calculate that GV02 uplifted 1.22 m between 16 April 2005 and the start of the eruption on 22 October 2005. This brings the precursory

*Deceased

[1]GSA Data Repository item 2006224, supplementary information on CGPS data processing, displacement vectors, and models used in the study, is available online at www.geosociety.org/pubs/ft2006.htm, or on request from editing@geosociety.org or Documents Secretary, GSA, P.O. Box 9140, Boulder, CO 80301-9140, USA.

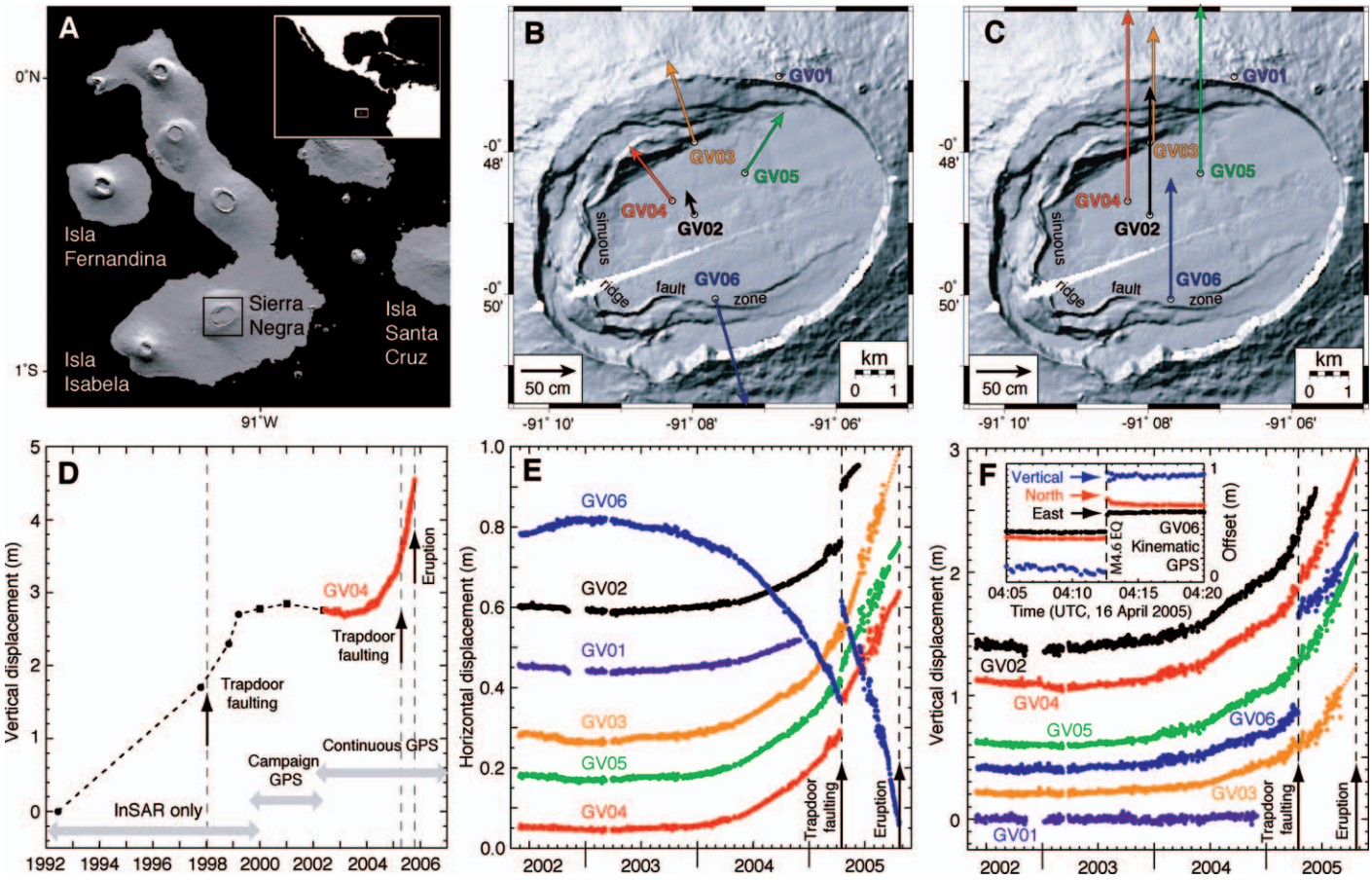

Figure 1. Continuous global positioning system (CGPS) results showing pre-eruption deformation at Sierra Negra volcano. A: Location map after Yun el al. (2006). B: Summit of Sierra Negra, showing sinuous ridge fault system, location of CGPS stations, and horizontal displacements during inflation from 1 April 2003 to 21 October 2005 (GV01 only to 3 December 2004; GV02 only to 10 June 2005). Fault-related displacements on 16 April 2005 are not included (see Fig. 2). C: Vertical displacements during inflation, as in B. D: Uplift history of center of caldera at Sierra Negra from 1992 to 2006 amounting to nearly 5 m. Times of major trapdoor faulting events and 2005 eruption are indicated. E: Horizontal displacements (north component only) at CGPS stations from 2002 to 2006, relative to stations GALA and GLPS on Isla Santa Cruz. Noise level increases after 10 June 2005, when both dual-frequency receivers had failed (GV01 and GV02). After 1 September 2005, GALA and GLPS were also down; thereafter movement at GV03 is extrapolated (dashed line) and GV04, GV05, and GV06 are shown relative to GV03. F: Vertical displacement time series, as in E. Inset shows kinematic solution for displacements at GV06 during 16 April 2005 trapdoor faulting event, relative to GV03. Vertical dashed lines in E and F show times of 16 April 2005 trapdoor faulting event and eruption on 22 October 2005. InSAR—inferometric synthetic aperture radar; GPS—global positioning system.

uplift to 2.20 m at GV02 from 1 April 2003 to 22 October 2005. Note, however, that station GV02 failed on 10 June 2005 and its vertical displacement between then and the eruption on 22 October 2005 is estimated by adding 20% to the uplift measured at nearby station GV04 during this time interval, the previous average difference between the two stations. This extrapolation is not used in the figures or in the modeling discussed here. Horizontal extension across the caldera (GV03–GV06) amounted to 97 cm between 16 April 2005 and the eruption, and a total of 1.4 m since 1 April 2003 (Fig. 1).

Interferograms made from radar scenes collected by the European Space Agency's ENVISAT satellite were examined to more fully document the spatial pattern of deformation at Sierra Negra since early 2004 (Fig. 2; Data Repository [see footnote 1]). The topographic correction used in making the interferograms is based on a merged Shuttle Radar Topography Mission (SRTM) and Topographic Synthetic Aperature Radar (TOPSAR) digital elevation model by Yun et al. (2005). One interferogram (12 February 2004–27 January 2005) shows 0.55 m of maximum radar line of sight (LOS) shortening due to caldera-wide inflation centered ~800 m SE of GV02 (Fig. 2A). A second interferogram (27 January 2005–12 May 2005), which includes the 16 April 2005 faulting event, shows a maximum LOS shortening of 1.0 m along the intracaldera fault system close to GV06 and a loss of coherence phase across the fault system (Fig. 2B). Note that ~4 months of inflation signal is superimposed on the instantaneous fault displacements in the second interferogram.

MODELING

The elastic bulging of the caldera floor leading up to the 2005 eruption is almost certainly due to intrusion of magma into a sill beneath the caldera that has been previously modeled at a depth of ~2 km (Amelung et al., 2000; Geist et al., 2006; Yun et al., 2006). Using InSAR and CGPS data from 12 February 2004 to 27 January 2005 (Data Repository; see footnote 1), we obtain a sill depth of 2.2 km and find that the sill volume was increasing at a rate of 17×10^6 m^3/yr. The average rate of volume increase before the trapdoor faulting (1 April 2003–15 April 2005) was 14×10^6 m^3/yr, based on CGPS data and using the same sill geometry, whereas the average rate between the trapdoor faulting and the eruption (16 April 2005–21 October 2005) was much higher at 64×10^6 m^3/yr.

The 2004–2005 interferograms are remarkably similar to the pattern of deformation documented by InSAR in the 1990s (Amelung et al., 2000; Jónsson et al., 2005). Despite these similarities, our modeling results of the 2005 faulting event differ significantly from the previous interpretations of the 1997–1998 event. In order to isolate the motions

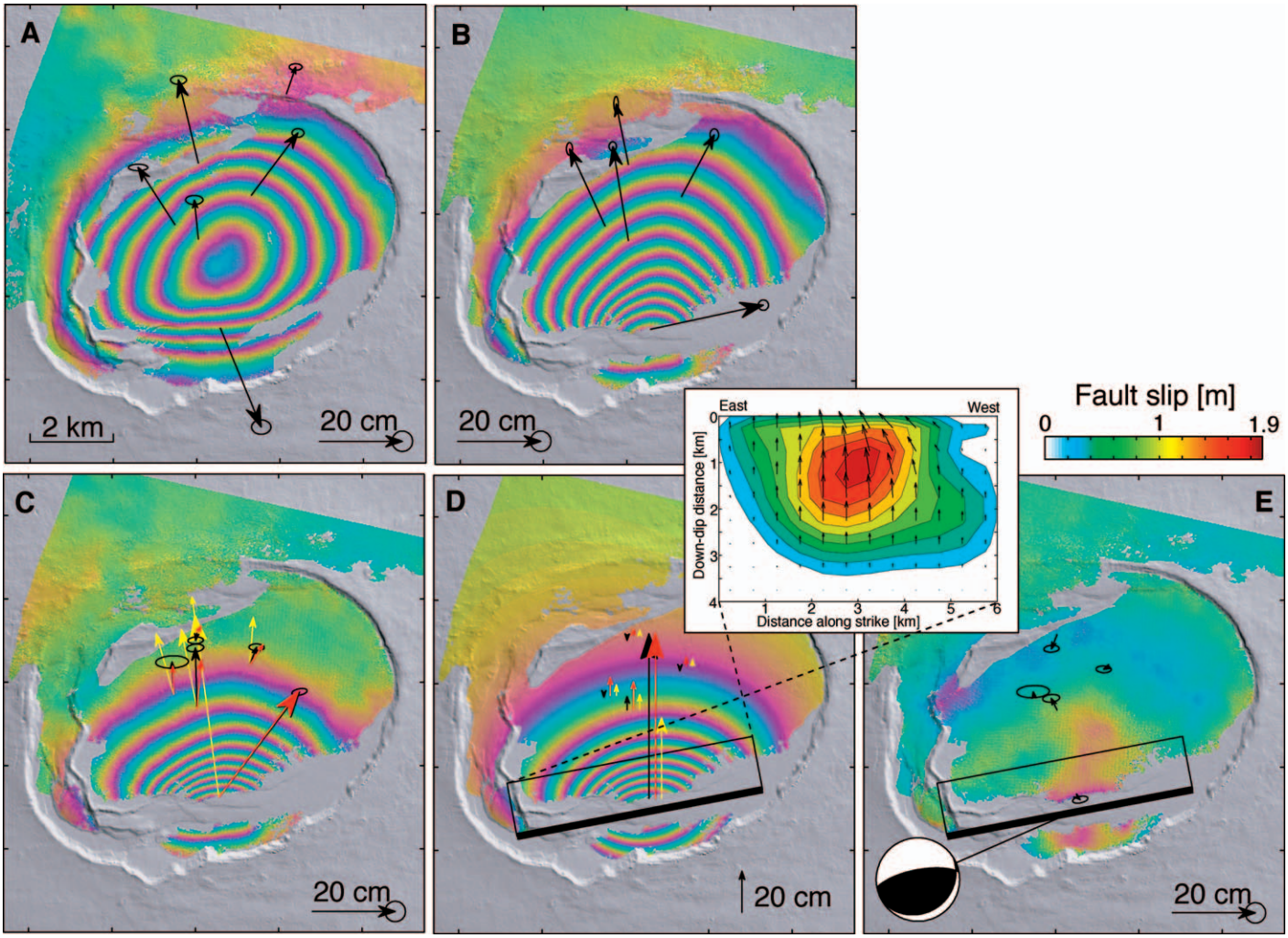

Figure 2. Inferometric synthetic aperture radar (InSAR) and continuous global positioning system (CGPS) data and comparison with trapdoor fault models. A: InSAR observations and horizontal CGPS displacements indicating uplift from 12 February 2004 to 27 January 2005. InSAR data are displayed at 10 cm range change per fringe. B: InSAR and CGPS observations from 27 January 2005 to 12 May 2005 showing effect of both uplift and trapdoor faulting. C: Same InSAR observations as in B, but corrected for deformation related to uplift and effectively only showing deformation due to trapdoor faulting on 16 April 2005. Black and red vectors show observed and predicted horizontal displacements, respectively. Yellow vectors in C and D show predicted displacements from model of Amelung et al. (2000). D: Simulated interferogram from our trapdoor fault model (inset). Black and red vectors show observed and predicted vertical displacements, respectively. E: Residual between InSAR data in C and model prediction in D with residual horizontal CGPS displacements. Focal mechanism shows modeled sense of slip.

due to the trapdoor faulting event, it is assumed that the pattern of inflation captured in the first interferogram (12 February 2004–27 January 2005) continued until the time of faulting and after faulting took place. This pattern of uplift was scaled by the CGPS data and then subtracted from the second interferogram, yielding an interferogram that effectively isolates the deformation signal of the trapdoor faulting event on 16 April 2005 (Fig. 2C).

In a joint inversion of the fault-related CGPS and InSAR displacements (Jónsson et al., 2002), we solve for both the fault geometry and slip, and find that the best-fit elastic dislocation model (Data Repository; see footnote 1) is a high-angle reverse fault with a strike of 259° and a dip of 71° north (Figs. 2C–2E). Dip slip alone cannot match the horizontal displacements at GV06, and a small component of right-lateral strike-slip motion is required. When allowing for variable fault slip, we find maximum reverse faulting of 1.9 m, and right-lateral strike slip at shallow depths accounts for ~13% of the total geodetic moment (Fig. 2D). No evidence for inelastic deformation or site instability was found when the GV06 site was examined after the earthquake.

Amelung et al. (2000) used south-dipping normal faults and a four segment fault geometry that mimicked the surface trace of the fault system to model the 1997–1998 trapdoor faulting event. However, we found that this geometry could not match the observed CGPS displacements in 2005 (Fig. 2). We conclude that the 1997–1998 trapdoor event also occurred on a north-dipping reverse fault, because a model similar to the one in Figure 2 can also fit the 1997–1998 InSAR data (see Data Repository). This clearly demonstrates that using GPS and InSAR together provides more robust model constraints than using either data set alone.

DISCUSSION

Although a sparse seismic network exists in Galápagos, it was not operational during 2003–2005 and only data from the global network are available. The 16 April 2005 earthquake had a magnitude of m_b4.6 (National Earthquake Information Center; http://neic.usgs.gov). A simple calculation of the moment based on the preferred dislocation model is 5×10^{17} Nm (Kanamori and Anderson, 1975), equivalent to an M_w5.8 earthquake, assuming a shear modulus of 30 GPa. The discrepancy between geodetic and seismic moments, which was also observed associated with the 1997–1998 faulting event (presumed to be related to an M_w5.0 earthquake on 11 January 1998), could be caused by an

aseismic component to fault slip (Amelung et al., 2000). However, CGPS data from the 16 April 2005 earthquake (Data Repository; see footnote 1) clearly show that the fault slip was instantaneous (Fig. 1F). Therefore, we propose that the discrepancy may be caused by a combination of the underestimation of seismic magnitude from using body waves (m_b), as well as a lower elastic modulus and seismic attenuation in the shallow crust at Sierra Negra.

Although the 16 April 2005 earthquake is the clearest example, other earthquakes detected in the months preceding the October 2005 eruption (National Earthquake Information Center; http://neic.usgs.gov) may represent slip on the intracaldera fault system. The m_b4.0 earthquake on 23 February 2005 was associated with 4 cm of horizontal displacement at GV06 and 1 cm at GV02, and the m_b4.6 earthquake on 19 September 2005 caused 2 cm of horizontal displacement at GV05 and GV06. In addition, InSAR data suggest that the 19 September 2005 earthquake may be associated with faulting ~2 km east of GV06. An M_w5.5 earthquake occurred just 3 h before the eruption began on 22 October 2005, unfortunately during a period when the CGPS network was down, so we have no information about its cause. This event may have been related to the start of magma intrusion that culminated in the eruption.

The peak rate of uplift observed at Sierra Negra before the 2005 eruption (~1 cm/day) is relatively high, but not unprecedented. Similar inflation rates were observed at Krafla volcano, Iceland, during its 1975–1984 rifting episode (Björnsson, 1985). However, the cumulative vertical displacement of nearly 5 m since 1992 at Sierra Negra is extraordinary and is apparently the largest caldera-wide precursory inflation ever measured at a basaltic volcano. Most intereruption inflation episodes at other well-monitored basaltic volcanoes, including Kilauea and Mauna Loa, Hawaii, and Krafla, Iceland, produce no more than 1.5 m of uplift (typically <1 m) and have durations that are usually <1 yr (Dvorak and Dzurisin, 1997; Newhall and Dzurisin, 1988). This implies that the strain imposed by ~1 m of inflation at those volcanoes is usually enough to cause intrusion of magma to the surface. However, at Sierra Negra the amount of uplift recorded by CGPS between April 2003 and October 2005 was 2.2 m, and if the previous InSAR results since 1992 are included, this total increases to 4.9 m. The total intereruption uplift could potentially be much more, because the amount of uplift between 1979 and 1992 is unknown. A rough estimate of the intrusive volume since 1992 is 130×10^6 m^3, based on a variable-opening sill model used to fit the 2004–2005 observations and simply scaled to a maximum uplift of 5 m.

The repeated episodes of trapdoor faulting are likely responsible for the extraordinary magnitude and duration of precursory inflation observed at Sierra Negra. Cyclic trapdoor faulting relieves some of the strain produced in the roof of the magma reservoir by inflation, and this effectively postpones the time when an eruption would otherwise occur. Trapdoor faulting is self-perpetuating: once faults are established, they are zones of weakness that repeatedly fail. The trapdoor faults apparently are located above the edges of the sill, a geometry predicted for fractures developing due to sill growth (Fialko et al., 2001). The fault scarps near the 1997–1998 and 2005 trapdoor events are 10–20 m high (Jónsson et al., 2005), and the western section of the intracaldera fault system has scarps >100 m high, formed by faulted, uplifted, and tilted lava flows (Fig. 1B) (Reynolds and Geist, 1995). Our results suggest that the sinuous ridge formed by incremental faulting during many trapdoor events, driven by the accumulation of magma in a shallow sill.

In hindsight, when the amount of inflation since the 16 April 2005 faulting event approached the level that had caused previous failures, it was a sign that another faulting event or an eruption was near. If it is established that this is a cyclic pattern, then it is possible that earthquakes and eruptions might be forecast at this volcano on the basis of uplift related to shallow intrusion. In any case, these data show that inflation, faulting, and eruption are intimately intertwined at Sierra Negra and deformation there is a window into subsurface processes that may have predictive value in the future.

ACKNOWLEDGMENTS

This research was supported by grants from the National Science Foundation Earth Sciences Program (EAR-9814312 and EAR-0004067), and in part by the National Oceanic and Atmospheric Administration Vents Program (Pacific Marine Environmental Laboratory contribution 2896). ENVISAT radar data were provided by the European Space Agency through Eurimage Research Club grant 151. The Charles Darwin Research Station and the Galápagos National Park Service provided invaluable logistical assistance. Karen Harpp, Terry Naumann, and Kim Whipple helped in the field. Warren Gallaher and Karl Feaux of UNAVCO installed the continuous global positioning system network at Sierra Negra and Jim Normandeau kept the data flowing. This paper is dedicated to the memory of our friend, colleague, and coauthor Daniel J. Johnson, who died just weeks before the 2005 eruption of Sierra Negra.

REFERENCES CITED

Amelung, F., Jónsson, S., Zebker, H., and Segall, P., 2000, Widespread uplift and 'trapdoor' faulting on Galapagos volcanoes observed with radar interferometry: Nature, v. 407, p. 993–996, doi: 10.1038/35039604.

Björnsson, A., 1985, Dynamics of crustal rifting in NE Iceland: Journal of Geophysical Research, v. 90, p. 10,151–10,162.

Breitkreuz, C., and Petford, N., eds., 2004, Physical geology of high-level magmatic systems: Geological Society [London] Special Publication 234, 262 p.

Chouet, B.A., 2003, Volcano seismology: Pure and Applied Geophysics, v. 160, p. 739–788, doi: 10.1007/PL00012556.

Dvorak, J.J., and Dzurisin, D., 1997, Volcano geodesy: The search for magma reservoirs and the formation of eruptive vents: Reviews of Geophysics, v. 35, p. 343–384, doi: 10.1029/97RG00070.

Dzurisin, D., 2003, A comprehensive approach to monitoring volcano deformation as a window on the eruption cycle: Reviews of Geophysics, v. 41, p. 1001, doi: 10.1029/2001RG000107.

Fialko, Y., Khazan, Y., and Simons, M., 2001, Deformation due to a pressurized horizontal circular crack in an elastic half-space, with applications to volcano geodesy: Geophysical Journal International, v. 146, p. 181–190, doi: 10.1046/j.1365-246X.2001.00452.x.

Geist, D.J., Chadwick, W.W., Jr., and Johnson, D.J., 2006, Results from new GPS monitoring networks at Fernandina and Sierra Negra volcanoes, Galapagos, 2000–2002: Journal of Volcanology and Geothermal Research, v. 150, p. 79–97, doi: 10.1016/j.jvolgeores.2005.07.003.

Hugentobler, U., Schaer, S., and Fridez, P., 2001, Bernese GPS Software Version 4.2: Berne, Switzerland, University of Berne Astronomical Institute, 515 p.

Jónsson, S., Zebker, H., Segall, P., and Amelung, F., 2002, Fault slip distribution of the 1999 Mw7.1 Hector Mine earthquake, California, estimated from satellite radar and GPS measurements: Seismological Society of America Bulletin, v. 92, p. 1377–1389.

Jónsson, S., Zebker, H., and Amelung, F., 2005, On trapdoor faulting at Sierra Negra volcano, Galápagos: Journal of Volcanology and Geothermal Research, v. 144, p. 59–71, doi: 10.1016/j.jvolgeores.2004.11.029.

Kanamori, H., and Anderson, D.L., 1975, Theoretical basis of some empirical relations in seismology: Seismological Society of America Bulletin, v. 65, p. 1073–1095.

Marsh, B.D., 2004, A magmatic mush column Rosetta stone: The McMurdo Dry Valleys of Antarctica: Eos (Transactions, American Geophysical Union), v. 85, p. 497, 502.

Newhall, C.G., and Dzurisin, D., 1988, Historical unrest at large calderas of the world: U.S. Geological Survey Bulletin 1855, 1108 p.

Reynolds, R.W., and Geist, D.J., 1995, Petrology of lavas from Sierra Negra volcano, Isabela Island, Galápagos archipelago: Journal of Geophysical Research, v. 100, p. 24,537–24,553, doi: 10.1029/95JB02809.

Yun, S.-H., Ji, J., Zebker, H.A., and Segall, P., 2005, On merging high- and low-resolution DEMs from TOPSAR and SRTM using a prediction-error filter: Institute of Electrical and Electronics Engineers Transactions on Geoscience and Remote Sensing, v. 43, p. 1682–1690, doi: 10.1109/TGRS.2005.848415.

Yun, S.-H., Segall, P., and Zebker, H.A., 2006, Constraints on magma chamber geometry at Sierra Negra Volcano, Galápagos Islands, based on InSAR observations: Journal of Volcanology and Geothermal Research, v. 150, p. 232–243, doi: 10.1016/j.jvolgeores.2005.07.009.

Manuscript received 21 March 2006
Revised manuscript received 20 June 2006
Manuscript accepted 26 June 2006

Printed in USA

GSA Data Repository Item 2006###
for Geology paper G22826 - Chadwick et al.
A volcano bursting at the seams: Inflation, faulting, and eruption at Sierra Negra Volcano, Galápagos

1. Notes about CGPS data processing and reference stations used during this study.

Ionospheric corrections and other CGPS data processing procedures used in this study are the same as used by Bartel et al. (2003).

Bartel, B.A., Hamburger, M.W., Meertens, C.M., Lowry, A.R., and Corpuz, E., 2003, Dynamics of active magmatic and hydrothermal systems at Taal volcano, Philippines, from continuous GPS measurements: Journal of Geophysical Research, v. 108, p. 2475, doi:10.1029/2002JB002194.

GALA was the closest IGNS GPS site to Sierra Negra, located at the Charles Darwin Research Station in Puerto Ayora on Santa Cruz island, until it died on 07-Nov-02. A temporary site GAL2 was in operation from 07-Jan-03 to 07-Mar-03, which was then replaced by a permanent replacement site renamed GLPS on 28-Mar-03. However, GLPS was down from 01-Sep-05 until after the 22-Oct-2005 eruption.

GV01 and GV02 are dual-frequency instruments; GV03, GV04, GV05, GV06 are single-frequency instruments.

GV01 is relative to GALA/GLPS until it failed on 01-Dec-04. GV02 is relative to GALA/GLPS until it failed on 10-Jun-05. The level of noise in the CGPS results increased after 10-Jun-05, because both local dual-frequency instruments were down. GV03 is relative to GV01 until 01-Dec-04, then relative to GLPS until 01-Sep-05. After 01-Sep-05, GV01, GV02, and GLPS were all down. Between 01-Sep-05 and 22-Oct-05, displacements at GV03 were extrapolated, based on the average rates between 11-Jul-05 and 01-Sep-05. GV04, GV05 and GV06 are relative to GV01 until 01-Jan-04, then relative to GLPS until 01-Sep-05, then relative to the extraplated-GV03 until 22-Oct-05.

Table DR1. Approximate positions of the CGPS stations at Sierra Negra volcano.

	GV01	GV02	GV03	GV04	GV05	GV06
Latitude (S)	00° 46.94’	00° 48.88’	00° 47.87’	00° 48.69’	00° 48.30’	00° 50.06’
Longitude (W)	91° 06.80’	91° 07.98’	91° 07.98’	91° 08.29’	91° 07.27’	91° 07.69’

2. CGPS displacement vectors shown in Figure 1b,c (in meters).

Table DR2. CGPS displacements in Figures 1b and 1c (in meters).

01-Apr-03 to 21-Oct-05 (excluding the 16-Apr-05 trapdoor faulting event)						
	GV01*	GV02†	GV03	GV04	GV05	GV06
North	0.065	0.220	0.744	0.494	0.552	-0.989
East	0.020	-0.075	-0.244	-0.389	0.354	0.290
Vertical	0.038	1.177	1.053	1.749	1.544	1.107

* GV01 to 01-Dec-04 only.
† GV02 to 10-Jun-05 only.

All displacements were calculated from CGPS daily positions calculated as 5-point averages.

3. CGPS displacement vectors shown in Figure 2 a, b, c (in meters).

Table DR3. CGPS displacements shown in Figure 2a (in meters).

12-Feb-04 to 27-Jan-05 (inflation only)						
	GV01*	GV02	GV03	GV04	GV05	GV06
North	0.065	0.220	0.744	0.494	0.552	-0.989
East	0.020	-0.075	-0.244	-0.389	0.354	0.290
Vertical	0.038	1.177	1.053	1.749	1.544	1.107

* GV01 to 01-Dec-04 only.

Table DR4. CGPS displacements shown in Figure 2b (in meters).

27-Jan-05 to 12-May-05 (inflation and faulting)						
	GV01	GV02	GV03	GV04	GV05	GV06
North		0.227	0.146	0.186	0.149	0.058
East		-0.038	-0.030	-0.086	0.079	0.271
Vertical		0.474	0.143	0.358	0.245	1.000

Table DR5. CGPS displacements shown in Figure 2c (in meters).

15-Apr-05 to 17-Apr-05 (faulting only)†						
	GV01	GV02	GV03	GV04	GV05	GV06
North		0.146	-0.019	0.078	0.042	0.253
East		-0.004	-0.003	-0.004	0.016	0.019
Vertical		0.066	-0.030	-0.006	-0.023	0.792

† Daily results processed by Gypsy.

4. Notes on the inflating sill model used in the paper.

The best-fit sill-model for the InSAR/CGPS uplift between 12-Feb-04 and 27-Jan-05 was determined in two steps. First, parameters of a horizontal sill with uniform opening were estimated to determine the depth of the sill, and it was found to be 2.2 km (see table below). In the second step we fixed the sill depth at 2.2 km and the sill orientation at N55°E (approximately along the major axis of the elliptically shaped caldera), expanded the sill length and width, and solved for variable opening, which resulted in up to 1.5 m of opening. The results are listed in the table below:

Table DR6. Parameters for the sill model.

	Depth (km)	Length (km)	Width (km)	Orientation	Opening (m)
Uniform opening	2.2	5.0	2.9	N70°E	1.1 m
Variable opening	2.2*	10.0*	6.0*	N55°E*	0 - 1.5 m

* Denotes parameters that were held fixed in the inversion calculation.

The results of the sill model inversion are shown in the figures below.

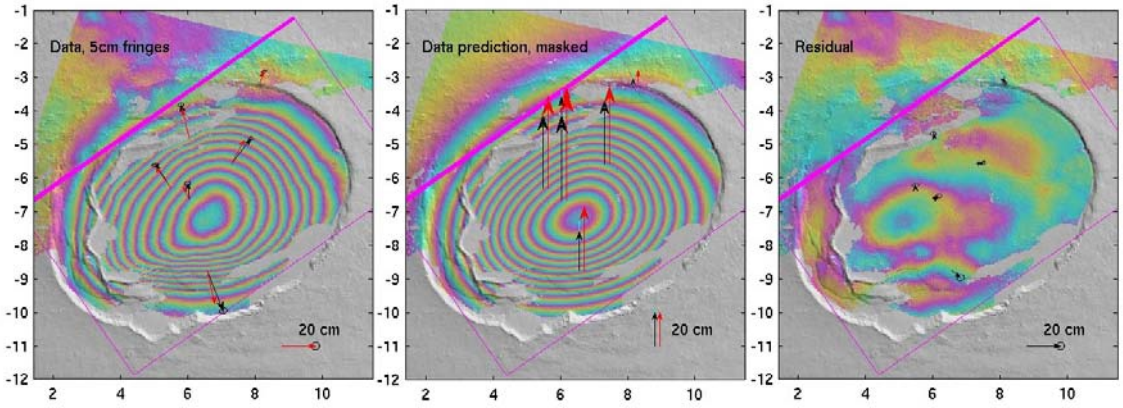

Figure DR1. InSAR data (left) in comparison with the sill model prediction (middle) and the residual (right) between the InSAR data and the model prediction. The InSAR data are displayed at 5 cm per color cycle, and represent the inflation between 12-Feb-04–27-Jan-05. The horizontal GPS data (black arrows) and model prediction (red) are shown on the left, the horizontal GPS residuals on the right, while the comparison of the vertical GPS measurements and model predictions are shown in the middle. Purple frame shows the outline of the 10 km x 6 km sill that was used in the estimation of the variable opening.

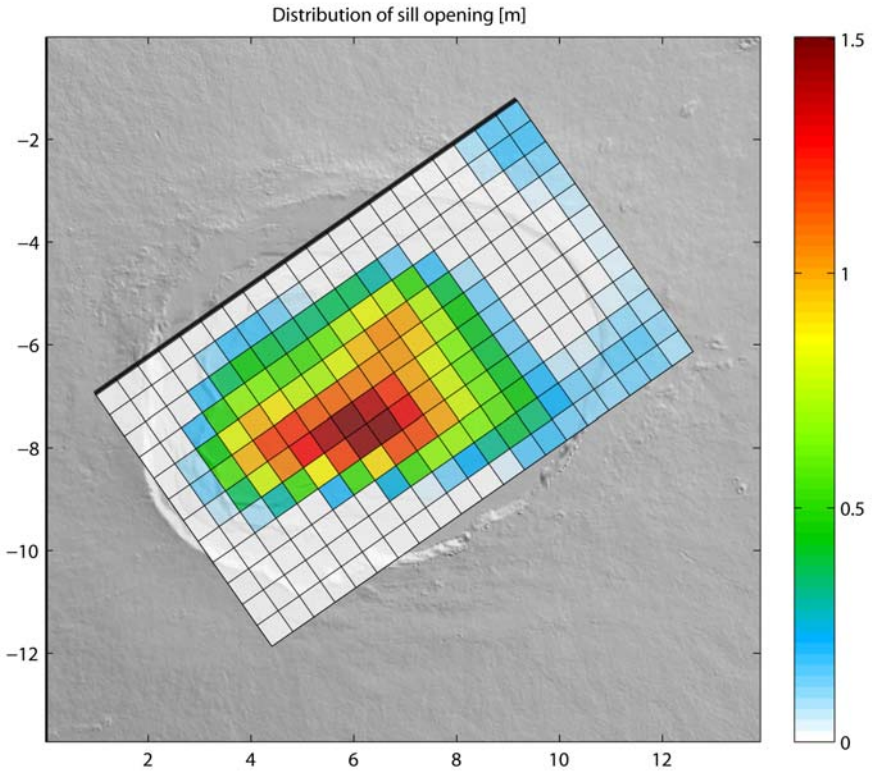

Figure DR2. Model results of variable opening of a sill at 2.2 km depth under Sierra Negra. The opening has a maximum of 1.5 m.

Note that in order to model the high fringe rate south of the uplift maximum, the sill opening has a very steep gradient south of the opening maximum, in comparison to other locations. It is interesting to speculate that there may be a barrier in the south, preventing the sill from propagating southward, resulting in this steep opening gradient. Perhaps this, in turn, results in high shear stresses in the sill roof at this location, promoting trapdoor faulting.

5. Notes on the fault modeling presented in the paper to fit displacements associated with the 16-Apr-2005 trapdoor faulting event.

We performed a joint inversion using both InSAR and CGPS data, as described in the paper. A non-linear optimization was carried out for the best-fit geometry of a single fault plane with 1) uniform dip-slip only, and 2) uniform slip with both dip- and strike-slip motion allowed. Then, we solved for spatially variable slip using fault parameters of the best fit fault #2.

The optimal fault geometry is almost exactly the same in the first two cases but the fit to CGPS station GV06 is greatly improved when strike-slip is included. The location, dimensions, and strike of the fault are constrained mostly by InSAR, whereas the dip, slip, and rake are constrained mainly by GPS. The best-fit model parameters are:

Table DR7. Best-fit parameters for fault models.

	Length (km)	Width (km)	Depth* (km)	Dip† (°)	Strike (°)	Strike slip (m)	Dip slip (m)	Rake (°)
Uniform-slip model (dip-slip only)	3.4	2.5	0.2	73	259	0.0	1.7	90
Uniform-slip model (dip-slip & strike-slip)	3.3	2.4	0.2	71	259	-0.6	1.5	111
Variable-slip model	6.0§	4.0§	0.0§	71§	259§	-0.9¶	1.9¶	97¶

* Depth is to upper edge of dipping fault plane.
† Dip is to the north (a reverse fault).
¶ These are maximum slip values and mean rake for the variable slip model
§ These parameters were held fixed in the inversion.

The resulting fault is a thrust that dips 71 degrees to the north. This differs from the trapdoor fault of Amelung et al. (2000) for the 1997-1998 event, which is a normal fault with a dip to the south (although we find the 1997-1998 data are better explained by a north-dipping fault - see later in this document). Therefore, the question here is: can we exclude all possible faults that dip to the south? To answer this question, we completed non-linear optimizations for different values of fault dip, and estimated optimal values for fault length, width, depth, strike, location, and slip in each case. We then investigated how the misfit changed as a function of fault dip and found that the weighted RMS misfit is 2 times higher for a fault dipping 71 degrees to the south, than for a fault dipping 71

degrees to the north. Faults that are nearly vertical, either dipping slightly to the south or to the north result in a smaller misfit, only about 1.2 times higher than the best fit fault, so it is harder to reject the possibility of a near vertical fault. This result does not depend on whether we estimate both dip-slip and strike-slip, or only dip-slip, components, nor on whether or not GPS station GV06 is included in the analysis.

Another way of looking at this problem is to estimate the model parameter confidence bounds from many model parameter optimizations using multiple realizations of the data covariance matrix. By doing this we find that the fault dip is statistically well constrained in the range of 68-74 degrees to the north (at a 95% confidence) and without strong trade-offs with other model parameters. The true fault-dip uncertainty is probably somewhat higher, as our confidence-bound calculation is based on only one possible fault model (i.e. single rectangular dislocation), and other fault-model scenarios (curving fault, multiple fault patches, etc.) would probably show a greater distribution of possible fault dips. However, based on our confidence interval calculation, we reject the possibility of a south dipping fault.

6. Notes on a revised trapdoor fault model that fits the 1997-8 InSAR data.

In the paper, we conclude that “the 1997-98 trapdoor event also occurred on a north dipping reverse fault, because a model similar to the one in Figure 2 can also fit the 1997-1998 InSAR data". This conclusion is based on the following:

The 1997-8 InSAR interferogram includes 13 months of inflation as well as the faulting, but in this case we cannot separate the two. However, we tried to do that using a method similar to the one we used in the paper for the 2005 faulting event. We removed

C x Uplift (12 Feb04 - 27 Jan 05)

from the 1997-8 interferogram, because the uplift pattern in 1992-7 and 1998-9 are very similar to the 2004-05 uplift pattern. The factor 'C' is estimated by trial and error. The resulting 'faulting only' signal for the 1997-8 event looks very similar to the 2005 event. The best fault dip for a simple (dip-slip only) fault is clearly dipping to the north, at 62°. A dip to the south has 2 times higher weighted RMS error. This result is also based on two major assumptions: (1) uplift can be removed, and (2) only dip-slip motion occurred. However, allowing for strike-slip motion also results in an optimal dip to the north. To deal with the uncertainty in removing the uplift, we also tried a combined inversion that allows for both faulting and sill opening. Here the optimal fault dip is closer to vertical, but still with a slight dip to the north. However, in this case, a range of fault dips can fit the data and there is not a significant difference in the weighted RMS error between solutions with fault dip of 75 degrees to the south to 40 degrees to the north. The reason is that here we invert for geometries of both a fault and a sill, and there are significant trade-offs between model parameters, most notably between fault dip and sill depth. For acceptable fault dips to the south the sill tends to be deep (~2.2 km), but for acceptable fault dips to the north it is shallower (~1.7-2.1 km).

Differences in the current modeling compared to the models of Amelung et al [2000] include: (1) one fault, instead of four, (2) Quadtree InSAR data sub-sampling, and (3) a full data covariance matrix.

7. Notes on daily vs. instantaneous (kinematic) displacements at GV06 during the 16-Apr-2005 trapdoor faulting event.

The daily and instantaneous displacements at GV06 associated with the 16-Apr-2005 trapdoor faulting event are similar.

Table DR8. Kinematic vs. daily CGPS displacements from the 16-Apr-05 faulting event.

	North displacement (m)	East displacement (m)	Vertical displacement (m)
Kinematic solution (10 sec)*	0.330	0.142	0.839
Kinematic solution (1 min)†	0.308	0.158	0.808
Daily solution (Bernese)†	0.240	0.195	0.788
Daily solution (Gypsy)†¶	0.253	0.193	0.792

* Displacements from single points (10 second epochs) before and after the earthquake (no averaging). These results are like the ones shown in the inset to Figure 1f in the paper.
† Displacements from 5-point averages before and after the earthquake.
¶ These are the results used in the fault modeling.

Therefore, it does not appear that there was significant post-seismic fault displacement following the earthquake. The differences between the kinematic and daily solutions are probably due to the relative inaccuracy of the kinematic solutions, rather than post-seismic displacement.